

Synthesis and QSAR analysis of chalcone derivatives as nitric oxide inhibitory agent

Kok Wai Lam · Reaz Uddin · Choi Yi Liew · Chau Ling Tham ·
Daud A. Israf · Ahmad Syahida · Mohd. Basyaruddin Abdul Rahman ·
Zaheer Ul-Haq · Nordin H. Lajis

Received: 3 June 2010 / Accepted: 11 June 2011 / Published online: 9 July 2011
© Springer Science+Business Media, LLC 2011

Abstract In this study, thirty-eight chalcone analogs were synthesized and evaluated for nitric oxide (NO) inhibition activity on RAW 264.7 cells. Among these compounds, chalcones bearing furanyl group showed remarkable anti-inflammatory activity. Both compounds **2d** and **2j** were identified as the most potent NO inhibitor on IFN- γ /LPS-activated RAW 264.7 cells. In order to examine the structure–activity relationship, a 3D QSAR analysis was carried out by comparative molecular field analysis (CoMFA) method on the selected chalcones. Partial least square analysis produced a statistically coherent model

with good predictive value, $r^2 = 0.989$ and a good cross validated value, $q^2 = 0.583$.

Keywords Nitric oxide inhibition · Chalcone analogues · RAW 264.7 · 3D QSAR · CoMFA

Introduction

Chalcone is a diarylpropanoid commonly found throughout the plant kingdom and acts as precursor for biosynthesis of flavonoids. Despite their structural simplicity, these compounds exhibit diverse important pharmacological effects on biological systems including anti-inflammatory (Correa *et al.*, 2001), anti-mycobacterial (Rojas *et al.*, 2002), anti-malarial (Chen *et al.*, 1994), anti-fungal (Boeck *et al.*, 2006; Lopez *et al.*, 2001), anti-viral (Phrutivorapongkul *et al.*, 2003), and anti-nociceptive (Correa *et al.*, 2001). Previous studies have shown that chalcones bearing phenyl group with chloro and hydroxyl substituents inhibit nitric oxide (NO) synthesis as well as inducible nitric oxide synthase (iNOS) protein expression in RAW 264.7 cells (Ko *et al.*, 2003; Won *et al.*, 2005). The synthetic chalcone 2',5'-dihydroxy-4-chlorodihydrochalcone was found to inhibit the cyclooxygenase-2 (COX-2) activity in RAW 264.7 cells (Huang *et al.*, 2001). In our own study on cardamonin, a naturally occurring chalcone isolated from the fruits of *Alpinia rafflesiana*, we found that it suppressed both NO and PGE₂ in interferon- γ (IFN- γ)- and lipopolysaccharide (LPS)- induced RAW 264.7 cells (Ahmad *et al.*, 2006; Israf *et al.*, 2007).

In order to explore further the interaction and effects of chalcone derivatives on inflammatory mediators, we synthesize further analogs of this class of compounds and establish the structure–activity relationship as the initial

K. W. Lam · N. H. Lajis (✉)
Laboratory of Natural Products, Institute of Bioscience,
University Putra Malaysia, 43400 UPM Serdang,
Selangor Darul Ehsan, Malaysia
e-mail: nhlajis@ibs.upm.edu.my

R. Uddin · Z. Ul-Haq
Dr. Panjwani Center for Molecular Medicine & Drug Research,
International Center for Chemical & Biological Sciences,
University of Karachi, Karachi 75270, Pakistan

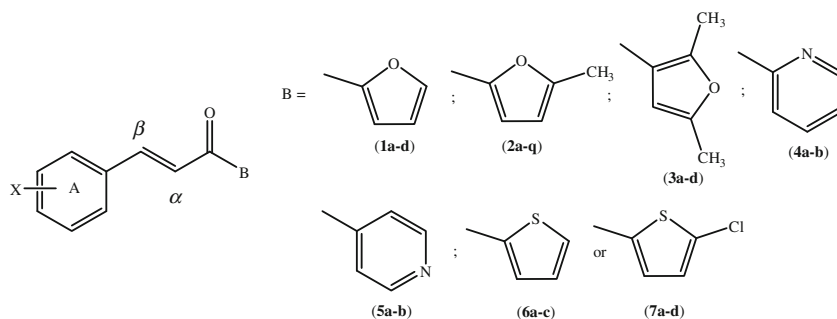
C. Y. Liew · C. L. Tham · D. A. Israf
Department of Biomedical Sciences,
Faculty of Medicine and Health Sciences,
University Putra Malaysia, 43400 UPM
Serdang, Selangor Darul Ehsan, Malaysia

A. Syahida
Department of Biochemistry,
Faculty of Biotechnology and Molecular Sciences,
University Putra Malaysia, 43400 UPM Serdang,
Selangor Darul Ehsan, Malaysia

Mohd. B. A. Rahman · N. H. Lajis
Department of Chemistry, Faculty of Science,
University Putra Malaysia, 43400 UPM Serdang,
Selangor Darul Ehsan, Malaysia

step. Three dimensional quantitative structure–activity relationship (3D QSAR) is an approach utilized in drug design. This approach is based on the physicochemical

Discussion



factors, steric and electrostatic field of the compound, and correlates them with biological activities. This effort is expected to allow us to understand the relationship between the physicochemical features of a compound with biological activities, and further design the more potentially effective drugs in a rational way. 3D QSAR analysis was applied to correlate the structure of chalcones and its biological activities have been reported (Chiaradia *et al.*, 2008; Liu and Go, 2007; Sivakumar *et al.*, 2007; Xue *et al.*, 2004). However, to the best of our knowledge, no 3D QSAR of chalcone and its NO inhibitory activity, as a preliminary investigation on its potential as anti-inflammatory agent, have not been undertaken.

Results

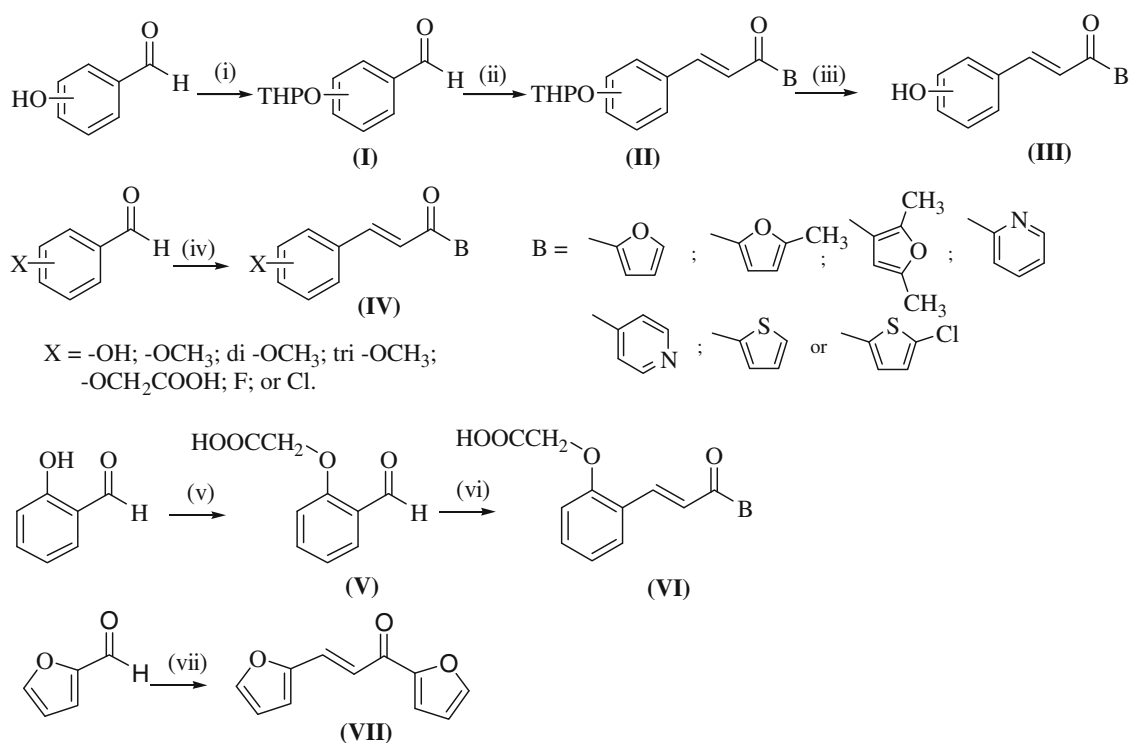
Synthesis

The general synthetic pathways for the preparation of the desired compounds are represented in Scheme 1. All chalcones were prepared based on Claisen-Schmidt condensation between the aromatic aldehydes and selected ketones. In general, the protection of hydroxylated aromatic aldehydes in the form of tetrahydropyranyl ether was required before base-catalyzed aldol condensation step. Deprotection using strong *p*-toluenesulfonic acid was conducted to achieve the desired respective products. However, this general strategy was not successful in the case of hydroxylated aromatic aldehyde at *ortho* position. The higher concentration of base with longer reflux time was required to accomplish satisfactory yields. Carboxymethylation of *para*-hydroxybenzaldehyde was accomplished by reacting it with α -chloroacetic acid in the presence of sodium hydroxide. All compounds were characterized by ^1H , ^{13}C NMR, EI-mass spectrometry and IR analysis.

Structure–activity relationship (SAR)

The NO inhibition activity of the synthesized chalcone derivatives on IFN- γ /LPS-activated macrophage cells is summarized in Table 1, with L-NAME used as positive control. The suppression of cell viability affected by all derivatives did not fall in close proximity to the IC_{50} of NO inhibition, and therefore, the inhibitory effect upon NO secretion was apparently not due to cell death. The results also clearly indicated that compounds exhibiting significant NO inhibitory activity may be related to the presence of aromatic rings (A and B) and a vinylketone moiety. The chalcones from series 2 exhibited higher NO suppression relative to other series with IC_{50} values ranging from 2.26 μM to more than 50 μM . The trend of NO inhibitory activity appeared to be in the order of $2 > 3 > 1 > 7 > 6 > 4 > 5$. One of the main reasons contributing to the striking effects of NO inhibition by compounds from series 2, 3, and 1 may be related to the presence of furanyl moiety in the compounds.

The NO suppression effect was further analyzed based on different theoretical parameters according to Lipinski criteria, which include logP, molecular weight and volume as well on the number of hydrogen bond donor and acceptor groups present (Lipinski *et al.*, 2001). Based on this analysis, all active NO inhibitors from series 2 recorded logP value of lower than 5, and thus fulfilled the Lipinski rules, which requires that most “drug-like” molecules should not exceed this value. Only compounds 2e and 2r from this series showed poor NO suppression. These chalcone analogs possessed low logP values, which is associated with their high hydrophilic character. This in turn may restrict their capability to cross the hydrophobic barrier in cells or in ligand binding in the active site. Similar instance was also observed in the case of series 4 and 5 compounds, which recorded a low logP values in the region of 2, and could be rationalized as to be due to the presence of pyridinyl ring (ring B). These compounds



Scheme 1 Synthetic scheme for chalcone analogs. Reagents and conditions: (i) 3,4-dihydro-2H-pyran, pyridinium *p*-toluenesulfonate, CH_2Cl_2 , 4 h. (ii) respective heterocyclic ketone, NaOH, ethanol, reflux. (iii) TsOH, methanol, rt, 2 h. (iv) respective aldehyde, respective

heterocyclic ketone, NaOH, ethanol, reflux. (v) α -chloroacetic acid, NaOH, reflux, 4 h. (vi) respective heterocyclic ketone, NaOH, ethanol, reflux. (vii) 2-acetylfuran, NaOH, ethanol, reflux

displayed only moderate NO inhibition activity. According to Lipinski, logP is an important feature for good drug absorption and permeation (Balanco *et al.*, 1998; Tetko *et al.*, 2005; Veber *et al.*, 2002).

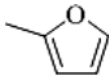
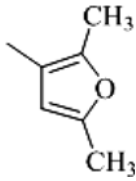
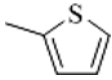
Correlating the structural feature of ring **B** with the activity revealed that furanyl radical generally recorded higher NO inhibitory activity than pyridinyl or thiophenyl analogs. Both of these compounds did not violate any of the Lipinski rules. Structurally, the only major difference is the replacement of oxygen with sulfur atom in the five-membered ring **B**. This observation could be best explained by the fact that the oxygen species in furan ring might have a higher hydrogen bond accepting capacity compared with the sulfur species in the thiophenyl derivatives. In the case of thiophene, H-bond formation is more susceptible toward the aromatic *pi* system as compared with the unshared electron pair localized at S atom. In contrast, the oxygen atom in the furanyl ring is more capable of forming hydrogen bond through its non-bonding electron pair (Cooke *et al.*, 1998). The pyridinyl derivatives from series **4** and **5** demonstrated minimal NO inhibition compared with the furanyl and thiophenyl series, which could be rationalized by the larger ring size of **B**, thus prohibiting its occupancy in the active site of the mediators in NO production.

On the other hand, the presence of electron donating group such as hydroxyl group at *ortho* position in the phenyl ring **A** appeared to be an important factor for NO suppression in the series **1**, **2**, **4**, **5**, **6**, and **7**. Analog **2a**, bearing *ortho*-hydroxyl group in ring **A** recorded significant suppression of nitrite with an IC_{50} value of $5.88 \pm 0.38 \mu M$, while **5a** recorded a lower activity with an IC_{50} value of $31.74 \pm 1.21 \mu M$. These results suggest that the presence of *ortho* phenolic hydroxyl group at ring **A** was vital for the suppression of NO secretion in RAW 264.7. This was further supported by the fact that replacing the proton of *ortho*-hydroxyl into an acetic acid group in compounds **2e** and **3d** totally masked the NO inhibition activity.

Among the compounds in series **3**, in which ring **B** consisted of 2,5-dimethylfuran ring, the highest NO suppression was observed when the hydroxyl substituent was located at *meta*-position at ring **A**. This was in contrast to the related compounds from series **2**. *m*-Hydroxylated phenyl ring in this group of compounds exhibited lower IC_{50} value than those analogs from series **1** and **2**. This change in activity trend may be related to the change of location of the oxygen atom in ring **B**, resulting in the alteration of their interaction with the mediators.

The results presented in Fig. 1 show that analogs **2j** and **2r** inhibited NO secretion in a dose-dependent manner. The most

Table 1 The IC₅₀ values of anti-inflammatory activity and the Lipinski's Rule of five values for chalcone derivatives

Compound (series)	Substituted position in phenyl ring A, X	Ring B	Anti-inflammatory activity IC ₅₀ (μM) (Mean ± SEM ^a)	Lipinski Rule of 5 ^b				
				miLogP	Volume	MW	HBA	HBD
1a	<i>o</i> -hydroxy		19.33 ± 2.82	2.829	191.438	214.220	3	1
1b	<i>m</i> -hydroxy		24.76 ± 2.64	2.565	191.438	214.220	3	1
1c	<i>p</i> -hydroxy		24.89 ± 3.29	2.589	191.438	214.220	3	1
1d	2,5-dimethoxy		16.02 ± 0.97	2.930	234.512	258.273	4	0
2a	<i>o</i> -hydroxy		5.88 ± 0.38	3.051	207.999	228.247	3	1
2b	<i>m</i> -hydroxy		9.35 ± 0.95	2.787	207.999	228.247	3	1
2c	<i>p</i> -hydroxy		16.29 ± 0.63	2.811	207.999	228.247	3	1
2d	2,5-dimethoxy		2.51 ± 0.42	3.152	251.073	272.300	4	0
2e	<i>o</i> -(2-oxyacetic acid)		≥50	2.365	252.769	286.283	5	1
			14.51 ± 1.34	3.249	223.315	257.245	5	0
2f	<i>p</i> -nitro		5.62 ± 1.52	3.137	276.618	302.326	5	0
2g	2,4,6-trimethoxy		4.47 ± 1.47	2.939	276.618	302.326	5	0
2h	2,3,4-trimethoxy		5.31 ± 0.60	3.259	230.458	260.264	3	0
2i	2-fluoro,4-methoxy		2.26 ± 0.47	2.931	251.073	272.300	4	0
2j	2,3-dimethoxy		6.45 ± 1.50	3.128	251.073	272.300	4	0
2k	2,6-dimethoxy		12.87 ± 2.45	3.226	204.913	230.238	2	0
2l	<i>o</i> -fluoro		16.06 ± 3.78	3.430	204.913	230.238	2	0
2m	<i>m</i> -fluoro							
2n	<i>p</i> -fluoro		17.04 ± 2.82	3.454	204.913	230.238	2	0
2o	<i>o</i> -chloro		16.98 ± 4.51	3.741	213.517	246.693	2	0
2p	<i>m</i> -chloro		7.76 ± 1.32	3.944	213.517	246.693	2	0
2q	<i>p</i> -chloro		11.48 ± 1.86	3.968	213.517	246.693	2	0
2r	Furan		21.31 ± 2.15	2.368	181.549	202.209	3	0
3a	<i>o</i> -hydroxy		13.78 ± 0.28	2.962	224.560	242.274	3	1
3b	<i>m</i> -hydroxy		7.96 ± 0.10	2.698	224.560	242.274	3	1
3c	<i>p</i> -hydroxy		13.50 ± 2.03	2.722	224.560	242.274	3	1
3d	<i>o</i> -(2-oxyacetic acid)		≥50	2.276	269.330	300.310	5	1
4a	<i>o</i> -hydroxy		29.95 ± 1.07	2.402	205.714	225.247	3	1
4b	<i>m</i> -hydroxy		49.51 ± 1.18	2.138	205.714	225.247	3	1
5a	<i>o</i> -hydroxy		31.74 ± 1.21	2.283	205.714	225.247	3	1
5b	<i>m</i> -hydroxy		≥50	2.019	205.714	225.247	3	1
5c	<i>p</i> -hydroxy		≥50	2.043	205.714	225.247	3	1
6a	<i>o</i> -hydroxy		16.22 ± 0.18	3.471	200.582	230.288	2	1
6b	<i>p</i> -hydroxy		46.82 ± 0.95	3.231	200.582	230.288	2	1
6c	2,5-dimethoxy		38.71 ± 0.24	3.572	243.656	274.341	3	0
7a	<i>o</i> -hydroxy		23.43 ± 1.02	4.273	214.118	264.733	2	1
7b	<i>m</i> -hydroxy		33.28 ± 1.63	4.009	214.118	264.733	2	1
7c	<i>p</i> -hydroxy		≥50	4.033	214.118	264.733	2	1
7d	2,5-dimethoxy		26.04 ± 0.83	4.374	257.191	308.786	3	0
9a	L-NAME ^c	–	23.21 ± 1.64	ND	ND	ND	ND	ND
8a	cardamomin	–	11.48 ± 1.25	3.233	243.434	270.284	4	2

ND not determined

^a Standard error of the mean

^b Calculation was generated out online www.molinspiration.com website (Molinspiration Property Engine v2009.01)

^c Positive control used for anti-inflammatory assay

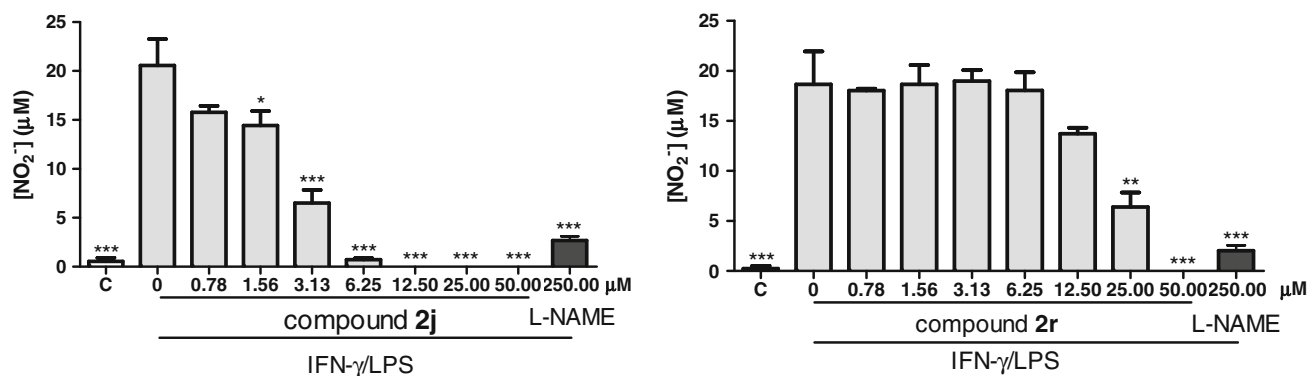


Fig. 1 Nitric oxide (NO) production level of RAW 264.7 in the presence of compounds **2j** and **2r**. C: basal level of nitrite concentration without IFN- γ /LPS treatment. All values are mean \pm SEM. of

three different experiments. * $P < 0.05$, ** $P < 0.01$, *** $P < 0.001$ significantly different from the IFN- γ /LPS-treated control group

active compound **2j** suppressed the NO production significantly, with an IC₅₀ value of $2.26 \pm 0.47 \mu\text{M}$, which represents almost a 10-fold and 5-fold improvement compared with positive inhibitor, L-NAME and cardamonin, respectively. Compound **2r** recorded less significant NO inhibition with an IC₅₀ value of $21.31 \pm 2.15 \mu\text{M}$, which suggested that a six-membered phenyl ring in **A** might be required for the NO inhibition. In another related study on compound **2j**, it was suggested that the NO inhibition was due to the down-regulation of inducible nitric oxide synthase (iNOS), and cyclooxygenase-2 (COX-2), without any direct effect upon iNOS or COX-2 enzyme activity (Liew *et al.* 2010).

Figure 2 represents the effect of compounds **2j** and **2r** upon the viability in RAW 264.7 cells. It is evident that compound **2j** is toxic to cells at the concentrations of 25 μM and above, whereas **2r** does not. Therefore, it was obvious that the large difference in toxicity between **2j** and **2r** could be associated with the substituent pattern in ring **A**. Thus, replacement of 2,3-dimethoxyphenyl ring with furanyl in radical **A** resulted in an improvement to cell viability below the 50 μM concentration level (Table 1).

CoMFA analysis

QSAR with CoMFA was widely used in correlating the activity with molecular structure utilizing a set of physicochemical parameters (Cramer *III et al.*, 1988). The results from the statistical and graphical analyses can be employed to optimize the efficacy and safety of drug candidates through structural modification of the active templates. In this study, CoMFA method was adopted with Partial Least Squares (PLS) regression on NO inhibitory effect toward IFN- γ /LPS-activated RAW 264.7. CoMFA analysis was performed on 22 selected compounds and 18 of them were assigned as training sets ($n = 18$), while the other four as test sets ($n = 4$). A predictive CoMFA model on the basis of the common substructure-based alignment was generated in Table 2 with the conventional correlation coefficient $r^2 = 0.963$ and cross-validation $q^2 = 0.583$, while both the steric and electrostatic fields contribute 71.7% and 28.3%, respectively (Table 3). The results showed that steric interaction played a major role in the NO inhibition activity. Finally, four test sets were assigned

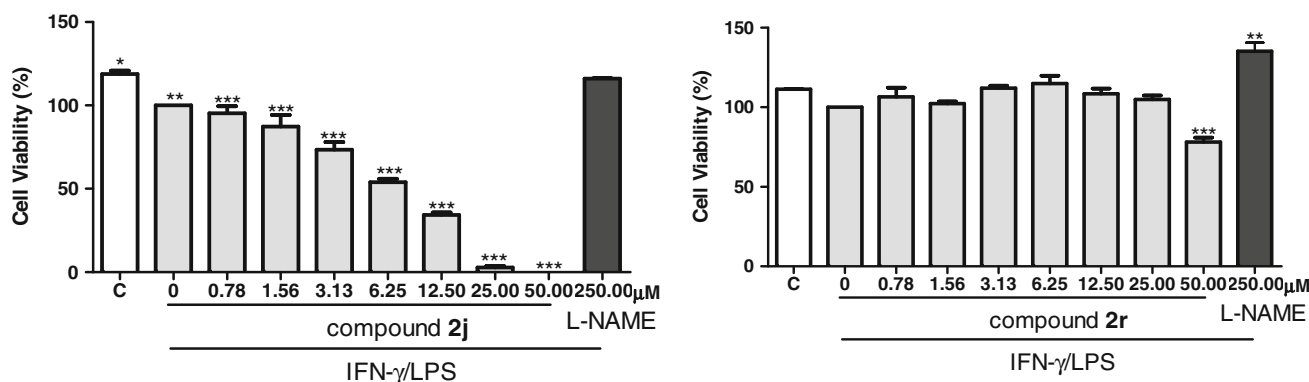


Fig. 2 RAW 264.7 cell viability in the presence of compounds **2j** and **2r**. C: basal level of nitrite concentration without IFN- γ /LPS treatment. All values are mean \pm SEM of three different experiments.

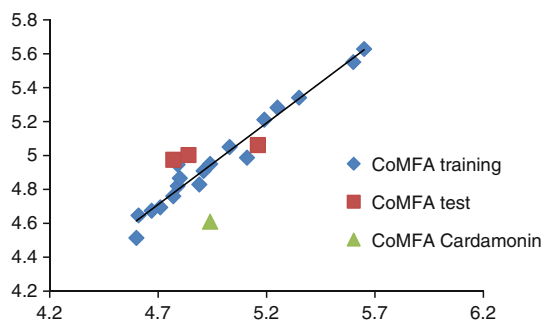
* $P < 0.05$, ** $P < 0.01$, *** $P < 0.001$ significantly different from the IFN- γ /LPS-treated control group

Table 2 Comparison of experimental and calculated biological activities of selected compounds by using CoMFA

No.	Compound	Actual pIC50	CoMFA predicted pIC50	Residual
Training set				
1	1a	4.71	4.69	0.02
2	1b	4.61	4.65	-0.04
3	1c	4.60	4.51	0.09
6	1d	4.80	4.87	-0.07
4	2b	5.03	5.05	-0.02
5	2c	4.79	4.82	-0.03
7	2d	5.60	5.55	0.05
8	2g	5.25	5.28	-0.03
9	2h	5.35	5.34	0.01
10	2i	4.91	4.91	0.00
11	2j	5.65	5.63	0.02
12	2k	5.19	5.21	-0.02
13	2l	4.89	4.83	0.06
14	2m	4.79	4.95	-0.15
15	2o	4.77	4.76	0.01
16	2p	5.11	4.99	0.12
17	2q	4.94	4.95	-0.01
18	2r	4.67	4.67	0.00
Test set				
19	2a	5.16	5.06	0.10
20	2f	4.84	5.00	-0.17
21	2n	4.77	4.98	-0.21
22	Cardamonin	4.94	4.61	0.33

to validate the reliability of the model as presented in Fig. 3.

The steric contour field map was plotted as shown in Fig. 4. The green isopleths represent the favorable steric group while the yellow isopleths represent the less favorable. The small-sized green-colored isopleths are found surrounding the methyl group in ring **B**. Green isopleths

**Fig. 3** Plots of the predicted versus experimental activity data of 3D-QSAR from CoMFA for the training and the test compounds

could also be found in the region of *ortho* position in ring **A**. For example, compounds in series **2**, which contain methyl group in the furanyl ring (radical **B**), displayed higher NO inhibition than compounds from series **1**. The prominent NO suppressive effects shown by those compounds containing methyl substituent in ring **B** proved to be an interesting new observation. These results also suggest that bulky substituent at this region is highly favorable for NO inhibition potency. Large-sized yellow-colored isopleths representing bulky favorable could be found in both *meta* positions in ring **A**.

The regions with red isopleths, which are defined as electrostatic favorable areas with negative charge could be found in the region of *ortho* and *para* position in ring **A**, suggesting that electron withdrawing groups in the *ortho* and *meta* position are highly favorable. A large-sized blue-colored isopleths encompassing the other side of *ortho* and *meta* position in ring **A**, suggesting that positive charge preference to enhance NO inhibition activity. Since most of the active compounds contain hydroxyl group in this blue region, it is therefore important to assume that the presence of electronegative atom in the *para* and *meta* position might be involved in the hydrogen bonding interaction with the target moieties in this region. For example, compounds **2d**, **2j**, and **2a** exhibited more potent NO inhibition than other compounds in the same series because of the presence of *ortho* hydroxy and methoxy group in ring **A**, which is necessary in affecting the NO suppression activity in the cell.

Experimental

Chemistry

All the chemicals and reagents were purchased from the suppliers including Sigma–Aldrich and Merck and Acros Organics chemical companies. All the solvents used in this experiment were either of HPLC-grade or dried and distilled before use. Typical work-ups include washing with brine and drying the organic layer with magnesium sulfate (anhydrous) followed by concentration in vacuo. Analytic TLC was carried out on silica gel F_{254} precoated (0.2 mm thickness, Merck) on aluminum sheets. The TLC plates were spotted with the samples using a fine glass capillary tube and developed in a chromatographic tank saturated with solvent vapor at room temperature. The IR spectra were recorded on a Perkin Elmer RXI FT-IR spectrometer as KBr disk or thin film. Mass spectra were measured on Thermo Finnigan POLARISQ spectrometer, with ionization induced by electron impact at 70 eV. Nuclear Magnetic Resonance Spectra were recorded in $CDCl_3$, CD_3OD , or $DMSO-d_6$ using Varian 500 MHz NMR Spectrometer.

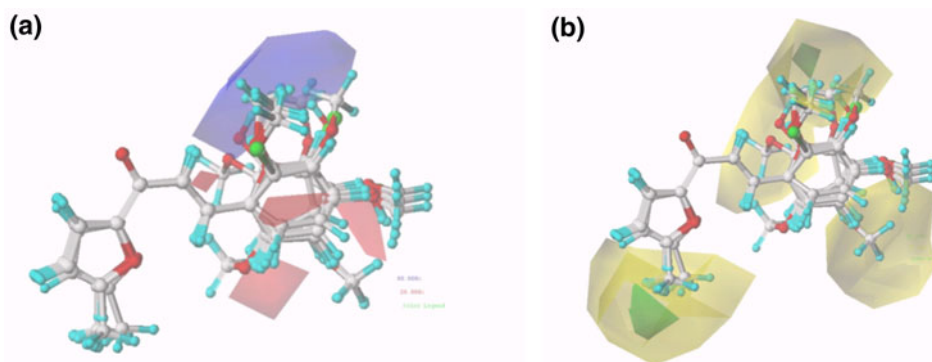


Fig. 4 Electrostatic and steric maps from the CoMFA model. **a** Favorable electrostatic areas with positive charges are indicated by blue isopleths, whereas favorable electrostatic areas with negative

charges are shown by red isopleths. **b** Favorable steric areas with more bulkiness are indicated by green isopleths, whereas the unfavorable steric areas are shown by yellow isopleths

Table 3 Summary of CoMFA analysis

CoMFA model	Result
R^2 cross validated (q^2)	0.583
SEP	0.254
Number of components	6
Non cross-validated r^2	0.963
Standard error of estimate	0.076
F	47.725
Steric contribution	0.717
Electostatic contribution	0.283
Predicted r^2	0.989
Predicted r^2 with cardamonin	0.126

General procedures for the synthesis of **I**

para- or *meta*-Hydroxylated aromatic aldehyde (10 mmol) was suspended in dichloromethane in the presence of pyridinium *p*-toluene sulfonate (10 mmol). The mixture was stirred at room temperature followed by the addition of 5 ml of 3,4-dihydropyran in dropwise manner. Then, the mixture was stirred monitored by TLC for another 4 h. Once the reaction was completed, the mixture was washed with water and extracted with ethyl acetate (EA). The EA layer was concentrated in vacuo, and the final product appeared as clear oils.

General procedures for the synthesis of **II**

A mixture of 10 mmol of **I** and 10 mmol of appropriate acetone (methyl heteroaryl ketone) in absolute ethanol was stirred, and a few drops of 40% of NaOH in ethanol was added. The mixture was stirred overnight at room temperature. The reaction was checked by TLC on the following day. After the reaction was completed, 50 ml of

water was added into the mixture, and the product was extracted with EA. The EA layer was concentrated in vacuo, and the final product was dried using magnesium sulfate anhydrous and used in the next step without further purification.

General procedures for the synthesis of **III**

The crude product from previous reaction (**II**) and catalytic amount of *p*-toluenesulfonic acid were dissolved in methanol. The mixture was stirred for 2 h, and the reaction was monitored by TLC. Once the reaction was completed, the mixture was washed with 40 ml water, neutralized with Na_2CO_3 and extracted with ethyl acetate. The organic layer was concentrated in vacuo and subjected to further purification using column chromatography.

General procedures for the synthesis of **IV**

Into a 150 ml single-necked round-bottomed flask containing a vigorously stirred mixture of appropriate aromatic aldehyde (10 mmol, 1 equiv) and ketone (10 mmol, 1 equiv) in 20 ml of absolute ethanol, a few drops of 40% NaOH in ethanol was slowly added. The stirring was continued and refluxed for 2 h. Upon completion, 100 ml of distilled water was added and further extracted with EA. The EA layer was concentrated in vacuo and subjected to further purification by recrystallization in appropriate solvent or column chromatography.

General procedures for the synthesis of **V**

A 20 ml aqueous solution of a mixture of 2-hydroxybenzaldehyde (10 mmol) and sodium hydroxide (20 mmol) was stirred, and α -chloroacetic acid (10 mmol) was added in a dropwise manner. The mixture was then heated under

reflux in a water bath for 4 h. Following this, the solution was acidified with 20 ml of concentrated hydrochloric acid and was cooled in ice bath. The white crystals **V** was formed and filtered off followed by rinsing with water. Further recrystallization was conducted from appropriate solvent. The reaction yielded a pure crystalline product.

General procedures for the synthesis of **VI**

The product **V** (10 mmol) was further reacted with selected 10 mmol of aldehyde in the presence of catalytic amount of 40% sodium hydroxide in 20 ml of absolute ethanol. The mixture was refluxed in a water bath for an hour. Water (50 ml) was then added, and the product was extracted with EA and concentrated in vacuo. The EA soluble extract was then subjected to purification using silica gel column chromatography.

General procedures for the synthesis of (**VII**)

Into a 150 ml single-necked round-bottomed flask containing a vigorously stirred mixture of appropriate aromatic aldehyde (10 mmol, 1 equiv) and ketone (10 mmol, 1 equiv) in 20 ml of absolute ethanol, a few drops of 40% NaOH in ethanol was slowly added. The stirring was continued and refluxed for 2 h. Upon completion, 100 ml of distilled water was added and further extracted with EA. The EA layer was concentrated in vacuo and subjected to further purification by recrystallization in appropriate solvent or column chromatography.

Spectral data

1-(furan-2-yl)-3-(2-hydroxyphenyl)prop-2-en-1-one (1a)
Yield: 42%; yellow crystals; IR(KBr) ν_{\max} : 3248 (–OH), 1644 (C=O), 1578 (C=C), 1459, 1052, 756; ^1H NMR (500 MHz, CD_3OD): δ 6.66 (dd, $J = 3.5/1.5$ Hz, 1H, H-3 furanyl), 6.86 (t, $J = 7.5$ Hz, 1H, H-5 phenyl), 6.88 (d, $J = 8.0$ Hz, 1H, H-3 phenyl), 7.23 (td, $J = 8.0/1.5$ Hz, 1H, H-4 phenyl), 7.46 (d, $J = 3.5$ Hz, 1H, H-4 furanyl), 7.63 (dd, $J = 7.5/1.5$ Hz, 1H, H-6 phenyl), 7.66 (d, $J = 16.0$ Hz, 1H, H- α), 7.81 (d, $J = 1.5$ Hz, 1H, H-2 furanyl), 8.18 (d, $J = 16.0$ Hz, 1H, H- β). ^{13}C NMR (125 MHz, CD_3OD): δ 112.6, 116.02, 118.4, 119.8, 120.6, 121.8, 129.3, 132.1, 140.5, 147.7, 153.8, 157.8, 179.3; EIMS m/z (rel. int.) calcd for $\text{C}_{13}\text{H}_{10}\text{O}_3$ (M^+ , %): 214 (M^+ , 8).

1-(furan-2-yl)-3-(3-hydroxyphenyl)prop-2-en-1-one (1b)
Yield: 56%; yellow crystals; IR(KBr) ν_{\max} : 3307 (–OH), 1654 (C=O), 1594 (C=C), 1460, 1278 (C–O aromatic), 1051, 765; ^1H NMR (500 MHz, CD_3OD): δ 6.69 (dd, $J = 3.5/1.5$ Hz, 1H, H-3 furanyl), 6.86 (d, $J = 8.0$ Hz, 1H, H-4 phenyl), 7.12 (s, 1H, H-2 phenyl), 7.19 (d, $J = 8.0$ Hz, 1H, H-6 phenyl), 7.52 (d, $J = 15.5$ Hz, 1H, H- α), 7.54 (d,

$J = 3.5$ Hz, 1H, H-4 furanyl), 7.76 (t, $J = 8.0$ Hz, 1H, H-5 phenyl), 7.84 (d, $J = 1.5$ Hz, 1H, H-2 furanyl), 8.12 (d, $J = 15.5$ Hz, 1H, H- β). ^{13}C NMR (125 MHz, CD_3OD): δ 112.7, 114.7, 118.0, 118.9, 120.2, 121.0, 130.0, 136.1, 144.5, 148.0, 153.6, 157.9, 178.6; EIMS m/z (rel. int.) calcd for $\text{C}_{13}\text{H}_{10}\text{O}_3$ (M^+ , %): 214 (M^+ , 74).

1-(furan-2-yl)-3-(4-hydroxyphenyl)prop-2-en-1-one (1c)
Yield: 50%; yellow powder; IR(KBr) ν_{\max} : 3430 (–OH), 1644 (C=O), 1572 (C=C), 1462, 1051, 826; ^1H NMR (500 MHz, CD_3OD): δ 6.69 (dd, $J = 3.5/1.5$ Hz, 1H, H-3 furanyl), 6.86 (d, $J = 8.5$ Hz, 2H, H-3/5 phenyl), 7.43 (d, $J = 15.5$ Hz, 1H, H- α), 7.52 (d, $J = 3.5$ Hz, 1H, H-4 furanyl), 7.61 (d, $J = 8.5$ Hz, 2H, H-2/6 phenyl), 7.80 (d, $J = 15.5$ Hz, 1H, H- β), 7.83 (d, $J = 1.5$ Hz, 1H, H-2 furanyl). ^{13}C NMR (125 MHz, CD_3OD): δ 112.6, 115.7, 115.8, 117.7, 118.3, 126.3, 130.8, 144.8, 147.7, 160.7, 178.9; EIMS m/z (rel. int.) calcd for $\text{C}_{13}\text{H}_{10}\text{O}_3$ (M^+ , %): 214 (M^+ , 69).

3-(2,5-dimethoxyphenyl)-1-(furan-2-yl)prop-2-en-1-one (1d)
Yield: 62%; IR(KBr) ν_{\max} : 2940 (C–H stretch), 1654 (C=O), 1594 (C=C), 1495 (C=C), 1464, 1260 (C–O aromatic), 1220, 1046; ^1H NMR (500 MHz, CDCl_3): δ 3.80 (s, 3H, OCH_3), 3.85 (s, 3H, OCH_3), 6.57 (dd, $J = 3.5/1.5$ Hz, 1H, H-3 furanyl), 6.87 (d, $J = 8.5$ Hz, 1H, H-3 phenyl), 6.94 (dd, $J = 8.5$ Hz/3.0 Hz, 1H, H-4 phenyl), 7.16 (d, $J = 3.0$ Hz, 1H, H-6 phenyl), 7.31 (d, $J = 3.5$ Hz, 1H, H-4 furanyl), 7.50 (d, $J = 16.0$ Hz, 1H, H- α), 7.64 (d, $J = 1.5$ Hz, 1H, H-2 furanyl), 8.17 (d, $J = 16.0$ Hz, 1H, H- β). ^{13}C NMR (125 MHz, CDCl_3): δ 50.0, 56.4, 112.6, 113.9, 117.6, 117.7, 122.2, 124.5, 126.4, 139.5, 146.6, 146.7, 153.7, 154.1, 178.7; EIMS m/z (rel. int.) calcd for $\text{C}_{15}\text{H}_{14}\text{O}_4$ (M^+ , %): 258 (M^+ , 12).

3-(2-hydroxyphenyl)-1-(5-methylfuran-2-yl)prop-2-en-1-one (2a)
Yield: 53%; orange needle crystals; IR(KBr) ν_{\max} : 3281 (–OH), 1640 (C=O), 1586 (C=C), 1511 (C=C), 1252 (C–O aromatic), 1073, 756; ^1H NMR (500 MHz, CD_3OD): δ 2.40 (s, 3H, CH_3), 6.30 (d, $J = 2.5$ Hz, 1H, H-4 furanyl), 6.85 (t, $J = 8.0$ Hz, 1H, H-5 phenyl), 6.89 (d, $J = 8.0$ Hz, 1H, H-3 phenyl), 7.23 (t, $J = 8.0$ Hz, 1H, H-4 phenyl), 7.39 (d, $J = 2.5$ Hz, 1H, H-3 furanyl), 7.59 (d, $J = 16.0$ Hz, 1H, H- α), 7.62 (d, $J = 8.0$ Hz, 1H, H-5 phenyl), 8.14 (d, $J = 16.0$ Hz, 1H, H- β). ^{13}C NMR (125 MHz, CD_3OD): δ 12.8, 109.4, 109.5, 115.9, 119.7, 120.7, 121.9, 129.1, 131.9, 139.8, 152.6, 157.7, 159.1, 178.6; EIMS m/z (rel. int.) calcd for $\text{C}_{14}\text{H}_{12}\text{O}_3$ (M^+ , %): 228 (M^+ , 12).

3-(3-hydroxyphenyl)-1-(5-methylfuran-2-yl)prop-2-en-1-one (2b)
Yield: 79%; yellow flakes; IR(KBr) ν_{\max} : 3306 (–OH), 1648 (C=O), 1593 (C=C), 1511 (C=C), 1282 (C–O aromatic), 1072, 783; ^1H NMR (500 MHz, CD_3OD): δ 2.42 (s, 3H, CH_3), 6.34 (d, $J = 3.0$ Hz, 1H, H-4 furanyl), 6.88 (dd, $J = 7.5$ Hz/1.5 Hz, 1H, H-4 phenyl), 7.12 (s, 1H, H-2 phenyl), 7.18 (dd, $J = 7.5/1.5$ Hz, 1H, H-6 phenyl),

7.26 (t, $J = 7.5$ Hz, 1H, H-5 phenyl), 7.46 (d, $J = 15.5$ Hz, 1H, H- α), 7.48 (d, $J = 3.0$ Hz, 1H, H-3 furanyl), 7.71 (d, $J = 15.5$ Hz, 1H, H- β). ^{13}C NMR (125 MHz, CD_3OD): δ 12.7, 109.3, 114.7, 117.8, 120.1, 121.1, 121.2, 129.9, 136.2, 143.8, 152.4, 157.9, 159.5, 177.8; EIMS m/z (rel. int.) calcd for $\text{C}_{14}\text{H}_{12}\text{O}_3$ (M^+ , %): 228 (M^+ , 32).

3-(4-hydroxyphenyl)-1-(5-methylfuran-2-yl)prop-2-en-1-one (2c); Yield: 68%; yellow amorphous; IR(KBr) ν_{max} : 3402 (O–H), 2956 (C–H stretch), 1676 (C=O), 1601 (C=C), 1520 (C=C), 1162, 833; ^1H NMR (500 MHz, DMSO): δ 2.31 (s, 3H, CH_3), 6.40 (d, $J = 3.0$ Hz, 1H, H-4 furanyl), 6.84 (d, $J = 8.5$ Hz, 2H, H-3 phenyl), 7.44 (d, $J = 15.5$ Hz, 1H, H- α), 7.60 (d, $J = 15.5$ Hz, 1H, H- β), 7.64 (d, $J = 3.0$ Hz, 1H, H-3 furanyl), 7.68 (d, $J = 8.5$ Hz, 2H, H-2 phenyl). ^{13}C NMR (125 MHz, DMSO): δ 14.4, 110.1, 116.5, 119.2, 121.2, 126.3, 131.5, 143.3, 152.8, 158.7, 160.7, 176.7; EIMS m/z (rel. int.) calcd for $\text{C}_{14}\text{H}_{12}\text{O}_3$ (M^+ , %): 228 (M^+ , 31).

3-(2,5-dimethoxyphenyl)-1-(5-methylfuran-2-yl)prop-2-en-1-one (2d) Yield: 69%; yellow crystals; IR(KBr) ν_{max} : 2945 (C–H stretch), 1652 (C=O), 1597 (C=C), 1514 (C=C), 1067, 802; ^1H NMR (500 MHz, DMSO): δ 2.39 (s, 3H, CH_3), 3.78 (s, 3H, OMe), 3.82 (s, 3H, OMe), 6.42 (d, $J = 3.5$ Hz, 1H, H-4 furanyl), 7.01 (overlapped, 2H, H-3/4 phenyl), 7.46 (s, 1H, H-6 phenyl), 7.63 (d, $J = 16.0$ Hz, 1H, H- α), 7.73 (d, $J = 3.5$ Hz, 1H, H-3 furanyl), 7.99 (d, $J = 16.0$ Hz, 1H, H- β). ^{13}C NMR (125 MHz, DMSO): δ 14.4, 56.2, 56.7, 109.9, 113.3, 113.6, 118.4, 121.9, 122.7, 124.1, 137.0, 152.7, 153.3, 153.9, 159.2, 176.6; EIMS m/z (rel. int.) calcd for $\text{C}_{16}\text{H}_{16}\text{O}_4$ (M^+ , %): 272 (30).

2-(2-(3-(5-methylfuran-2-yl)-3-oxoprop-1-enyl)phenoxy)acetic acid (2e) Yield: 43%; yellow powder; IR(KBr) ν_{max} : ^1H NMR (500 MHz, DMSO): δ 2.39 (s, 3H, CH_3), 4.83 (s, 2H, CH_2), 6.41 (d, $J = 3.5$ Hz, 1H, H-4 furanyl), 7.01 (overlapped, 2H, H-3/5 phenyl), 7.40 (t, $J = 8.0$ Hz, 1H, H-4 phenyl), 7.73 (overlapped, 2H, H-3 furanyl/H-6 phenyl), 7.82 (d, $J = 8.0$ Hz, 1H, H-4 phenyl), 7.90 (d, $J = 16.0$ Hz, 1H, H- β). ^{13}C NMR (125 MHz, DMSO): δ 14.3, 65.6, 109.9, 110.1, 113.3, 121.8, 123.5, 123.7, 130.8, 132.4, 138.0, 152.8, 157.5, 159.2, 170.7, 176.9; EIMS m/z (rel. int.) calcd for $\text{C}_{16}\text{H}_{14}\text{O}_5$ (M^+ , %): 211 (M^+ , 100).

1-(5-methylfuran-2-yl)-3-(4-nitrophenyl)prop-2-en-1-one (2f); Yield: 85%; orange crystals; IR(KBr) ν_{max} : 2922 (C–H stretch), 1640 (C=O), 1520 (C=C), 1340 (N–O), 1053, 1011; ^1H NMR (500 MHz, DMSO): δ 2.39 (s, 3H, CH_3), 6.39 (d, $J = 3.5$ Hz, 1H, H-4 furanyl), 6.74 (d, $J = 8.5$ Hz, 2H, H-2/6 phenyl), 7.36 (d, $J = 15.5$ Hz, 1H, H- α), 7.59 (overlapped, 3H, H-3 furanyl/H-3/4 phenyl), 7.64 (d, $J = 15.5$ Hz, 1H, H- β). ^{13}C NMR (125 MHz, DMSO): δ 14.3, 109.9, 112.4, 116.8, 120.4, 122.5, 131.2, 143.9, 152.6, 153.0, 158.2, 176.7; EIMS m/z (rel. int.) $\text{C}_{14}\text{H}_{11}\text{NO}_4$ (M^+ , %): 257 (M^+ , 100).

1-(5-methylfuran-2-yl)-3-(2,4,6-trimethoxyphenyl)prop-2-en-1-one (2g); Yield: 65%; yellow crystals; IR(KBr) ν_{max} : 2941 (C–H stretch), 1645 (C=O), 1588 (C=C), 1514 (C=C), 1321, 1206 (C–O aromatic), 1121, 755; ^1H NMR (500 MHz, DMSO): δ 2.39 (s, 3H, CH_3), 3.85 (s, 3H, OMe), 3.91 (s, 6H, OMe), 6.30 (s, 2H, H-3/5 phenyl), 6.38 (d, $J = 3.0$ Hz, 1H, H-4 furanyl), 7.37 (d, $J = 3.0$ Hz, 1H, H-3 furanyl), 7.65 (d, $J = 16.0$ Hz, 1H, H- α), 8.05 (d, $J = 16.0$ Hz, 1H, H- β). ^{13}C NMR (125 MHz, DMSO): δ 14.4, 56.2, 56.7, 91.6, 105.6, 109.9, 119.9, 120.9, 134.0, 153.1, 158.1, 162.0, 163.9, 178.0; EIMS m/z (rel. int.) calcd for $\text{C}_{17}\text{H}_{18}\text{O}_5$ (M^+ , %): 302 (M^+ , 5).

1-(5-methylfuran-2-yl)-3-(2,3,4-trimethoxyphenyl)prop-2-en-1-one (2h); Yield: 75%; yellow powder; IR(KBr) ν_{max} : 2939 (C–H stretch), 1651 (C=O), 1588 (C=C), 1514 (C=C), 1280 (C–O aromatic), 1096, 796; ^1H NMR (500 MHz, DMSO): δ 2.40 (s, 3H, CH_3), 3.79 (s, 3H, OMe), 3.86 (s, 3H, OMe), 3.91 (s, 3H, OMe), 6.41 (d, $J = 3.0$ Hz, 1H, H-4 furanyl), 6.91 (d, $J = 9.0$ Hz, 1H H-5 phenyl), 7.54 (d, $J = 16.0$ Hz, 1H, H- α), 7.65 (d, $J = 3.0$ Hz, 1H, H-3 furanyl), 7.69 (d, $J = 9.0$ Hz, 1H, H-6 phenyl), 7.86 (d, $J = 16.0$ Hz, 1H, H- β). ^{13}C NMR (125 MHz, DMSO): δ 14.4, 56.6, 61.0, 62.2, 109.1, 110.2, 121.1, 121.5, 124.0, 137.2, 142.5, 153.7, 156.3, 158.9, 176.7; EIMS m/z (rel. int.) calcd for $\text{C}_{17}\text{H}_{18}\text{O}_5$ (M^+ , %): 302 (M^+ , 12).

3-(2-fluoro-4-methoxyphenyl)-1-(5-methylfuran-2-yl)prop-2-en-1-one (2i); Yield: 87%; yellow crystals; IR(KBr) ν_{max} : 2921 (C–H stretch), 1652 (C=O), 1597 (C=C), 1513 (C=C), 1271 (C–O aromatic), 1067; ^1H NMR (500 MHz, DMSO): δ 2.40 (s, 3H, CH_3), 3.82 (s, 3H), 6.42 (d, $J = 3.5$ Hz, 1H, H-4 furanyl), 6.89 (d, $J = 12.0$ Hz, 1H, H-5 phenyl), 6.94 (d, $J = 12.0$ Hz, 1H, H-6 phenyl), 7.56 (d, $J = 16.0$ Hz, 1H, H- α), 7.67 (d, $J = 3.5$ Hz, 1H, H-3 furanyl), 7.73 (d, $J = 16.0$ Hz, 1H, H- β), 7.96 (s, 1H, H-3 phenyl). ^{13}C NMR (125 MHz, DMSO): δ 14.5, 56.6, 102.5, 110.1, 112.3, 115.2, 121.7, 130.7, 134.3, 152.6, 159.2, 161.7, 163.4, 162.7, 176.3; EIMS m/z (rel. int.) calcd for $\text{C}_{15}\text{H}_{13}\text{FO}_3$ (M^+ , %): 260 (M^+ , 39).

3-(2,3-dimethoxyphenyl)-1-(5-methylfuran-2-yl)prop-2-en-1-one (2j); Yield: 76%; yellow crystals; IR(KBr) ν_{max} : 2934 (C–H stretch), 1651 (C=O), 1596 (C=C), 1512 (C=C), 1267 (C–O aromatic), 1075, 999; ^1H NMR (500 MHz, DMSO): δ 2.40 (s, 3H, CH_3), 3.79 (s, 3H, OMe), 3.83 (s, 3H, OMe), 6.43 (d, $J = 3.0$ Hz, 1H, H-4 furanyl), 7.14 (overlapped, 2H, H-4/6 phenyl), 7.54 (t, $J = 4.5$ Hz, 1H, H-5 phenyl), 7.62 (d, $J = 16.5$ Hz, 1H, H- α), 7.72 (d, $J = 3.0$ Hz, 1H, H-3 furanyl), 7.95 (d, $J = 16.5$ Hz, 1H, H- β). ^{13}C NMR (125 MHz, DMSO): δ 14.4, 56.5, 61.7, 110.3, 115.6, 119.7, 122.1, 123.6, 124.9, 128.7, 136.8, 148.9, 152.6, 153.5, 159.3, 176.6; EIMS m/z (rel. int.) calcd for $\text{C}_{16}\text{H}_{16}\text{O}_4$ (M^+ , %): 272 (M^+ , 5).

3-(2,6-dimethoxyphenyl)-1-(5-methylfuran-2-yl)prop-2-en-1-one (**2k**) Yield: 82%; yellow needles; IR(KBr) ν_{\max} : 2942 (C–H stretch), 1649 (C=O), 1592 (C=C), 1513 (C=C), 1260 (C–O aromatic), 1203 (C–O), 1108, 742; ^1H NMR (500 MHz, DMSO): δ 2.40 (s, 3H, CH₃), 3.90 (s, 6H, OMe), 6.40 (d, $J = 3.0$ Hz, 1H, H-4 furanyl), 6.74 (d, $J = 8.0$ Hz, 2H, H-3/5 phenyl), 7.39 (t, $J = 8.0$ Hz, 1H, H-4 phenyl), 7.44 (d, $J = 3.0$ Hz, 1H, H-3 furanyl), 7.79 (d, $J = 16.0$ Hz, 1H, H- α), 8.09 (d, $J = 16.0$ Hz, 1H, H- β). ^{13}C NMR (125 MHz, DMSO): δ 14.4, 56.7, 104.8, 110.1, 112.0, 120.7, 124.1, 132.9, 133.7, 152.9, 158.6, 160.7, 177.9; EIMS m/z (rel. int.) calcd for C₁₄H₁₂O₃ (M⁺, %): 272 (M⁺, 4).

3-(2-fluorophenyl)-1-(5-methylfuran-2-yl)prop-2-en-1-one (**2l**); Yield: 84%; pale yellow powder; IR(KBr) ν_{\max} : 3111 (C–H stretch), 1660 (C=O), 1604 (C=C), 1513 (C=C), 1228 (C–O aromatic), 757; ^1H NMR (500 MHz, DMSO): δ 2.40 (s, 3H, CH₃), 6.43 (d, $J = 3.0$ Hz, 1H, H-4 furanyl), 7.29 (d, $J = 8.0$ Hz, 1H, H-3 phenyl), 7.30 (d, $J = 8.0$ Hz, 1H, H-6 phenyl), 7.49 (t, $J = 8.0$ Hz, 1H, H-5 phenyl), 7.70 (d, $J = 15.5$ Hz, 1H, H- α), 7.72 (d, $J = 3.0$ Hz, 1H, H-3 furanyl), 7.79 (d, $J = 15.5$ Hz, 1H, H- β), 8.03 (t, $J = 8.0$ Hz, 1H, H-4 phenyl). ^{13}C NMR (125 MHz, DMSO): δ 14.4, 110.4, 116.7, 122.4, 122.8, 124.8, 125.6, 129.7, 133.2, 134.1, 152.4, 159.6, 160.5, 176.1; EIMS m/z (rel. int.) calcd for C₁₄H₁₁FO₂ (M⁺, %): 230 (M⁺, 100).

3-(3-fluorophenyl)-1-(5-methylfuran-2-yl)prop-2-en-1-one (**2m**); Yield: 91%; yellow crystals; IR(KBr) ν_{\max} : 3104 (C–H stretch), 1654 (C=O), 1606 (C=C), 1513 (C=C), 1266 (C–O aromatic), 1068, 784; ^1H NMR (500 MHz, DMSO): δ 2.40 (s, 3H, CH₃), 6.43 (d, $J = 3.5$ Hz, 1H, H-4 furanyl), 7.26 (t, $J = 8.5$ Hz, 1H, H-5 phenyl), 7.49 (d, $J = 8.5$ Hz, 1H, H-4 phenyl), 7.64 (d, $J = 8.5$ Hz, 1H, H-5 phenyl), 7.67 (s, 1H, H-2 phenyl), 7.69 (d, $J = 15.5$ Hz, 1H, H- α), 7.77 (d, $J = 15.5$ Hz, 1H, H- β), 7.79 (d, $J = 3.5$ Hz, 1H, H-3 furanyl). ^{13}C NMR (125 MHz, DMSO): δ 14.5, 110.3, 115.2, 117.8, 122.5, 124.2, 126.1, 131.4, 137.9, 141.3, 152.5, 159.5, 164.2, 176.2; EIMS m/z (rel. int.) calcd for C₁₄H₁₁FO₂ (M⁺, %): 230 (M⁺, 68).

3-(4-fluorophenyl)-1-(5-methylfuran-2-yl)prop-2-en-1-one (**2n**) Yield: 72%; pale yellow powder; IR(KBr) ν_{\max} : 3017 (C–H stretch), 1650 (C=O), 1595 (C=C), 1511 (C=C), 1336 (C–O aromatic), 1067, 831; ^1H NMR (500 MHz, DMSO): δ 2.40 (s, 3H, CH₃), 6.44 (d, $J = 3.0$ Hz, 1H, H-4 furanyl), 7.31 (d, $J = 8.5$ Hz, 2H, H-3/5 phenyl), 7.62 (d, $J = 15.5$ Hz, 1H, H- α), 7.71 (d, $J = 15.5$ Hz, 1H, H- β), 7.75 (d, $J = 3.0$ Hz, 1H, H-3 furanyl), 7.93 (d, $J = 8.5$ Hz, 2H, H-2/6 phenyl). ^{13}C NMR (125 MHz, DMSO): δ 14.4, 110.2, 116.5, 122.2, 122.6, 131.8, 141.6, 152.6, 159.3, 163.0, 165.0, 176.4; EIMS m/z (rel. int.) calcd for C₁₄H₁₁FO₂ (M⁺, %): 230 (67).

3-(2-chlorophenyl)-1-(5-methylfuran-2-yl)prop-2-en-1-one (**2o**) Yield: 80%; pale yellow; IR(KBr) ν_{\max} : 3017

(C–H stretch), 1653 (C=O), 1600 (C=C), 1508 (C=C), 1335 (C–O aromatic), 1072, 760; ^1H NMR (500 MHz, DMSO): δ 2.40 (s, 3H, CH₃), 6.45 (d, $J = 3.5$ Hz, 1H, H-4 furanyl), 7.45 (overlapped, 2H H-4/5 phenyl), 7.55 (d, $J = 8.0$ Hz, 1H H-6 phenyl), 7.70 (d, $J = 15.5$ Hz, 1H, H- α), 7.78 (d, $J = 3.0$ Hz, 1H, H-3 furanyl), 7.99 (d, $J = 15.5$ Hz, 1H, H- β), 8.12 (d, $J = 8.0$ Hz, 1H, H-3 phenyl). ^{13}C NMR (125 MHz, DMSO): δ 14.4, 110.3, 122.9, 125.4, 128.4, 129.0, 130.7, 132.6, 132.8, 134.9, 137.4, 152.4, 159.8, 176.0; EIMS m/z (rel. int.) calcd for C₁₄H₁₁ClO₂ (M⁺, %): 246 (M⁺, 8).

3-(3-chlorophenyl)-1-(5-methylfuran-2-yl)prop-2-en-1-one (**2p**) Yield: 77%; yellow powder; IR(KBr) ν_{\max} : 2930 (C–H stretch), 1656 (C=O), 1602 (C=C), 1512 (C=C), 1205 (C–O aromatic), 1066; ^1H NMR (500 MHz, DMSO): δ 2.40 (s, 3H, CH₃), 6.44 (d, $J = 3.0$ Hz, 1H, H-4 furanyl), 7.47 (overlapped, 2H, H-4/5 phenyl), 7.64 (d, $J = 15.5$ Hz, 1H, H- α), 7.70 (d, $J = 15.5$ Hz, 1H, H- β), 7.81 (overlapped, 2H, H-3 furanyl/H-6 phenyl), 7.98 (s, 1H, H-2 phenyl). ^{13}C NMR (125 MHz, DMSO): δ 14.5, 110.3, 122.7, 124.3, 128.3, 128.5, 130.7, 131.4, 134.5, 137.5, 141.1, 152.5, 159.6, 176.2; EIMS m/z (rel. int.) calcd for C₁₄H₁₁ClO₂ (M⁺, %): 246 (M⁺, 99).

3-(4-chlorophenyl)-1-(5-methylfuran-2-yl)prop-2-en-1-one (**2q**) Yield: 89%; pale yellow powder; IR(KBr) ν_{\max} : 3011 (C–H stretch), 1650 (C=O), 1596 (C=C), 1508 (C=C), 1333 (C–O aromatic), 1065, 776; ^1H NMR (500 MHz, DMSO): δ 2.40 (s, 3H, CH₃), 6.44 (d, $J = 3.5$ Hz, 1H, H-4 furanyl), 7.51 (d, $J = 8.5$ Hz, 2H, H-3/5 phenyl), 7.66 (d, $J = 15.5$ Hz, 1H, H- α), 7.68 (d, $J = 15.5$ Hz, 1H, H- β), 7.76 (d, $J = 3.5$ Hz, 1H, H-3 furanyl), 7.87 (d, $J = 8.5$ Hz, 2H, H-2/6 phenyl). ^{13}C NMR (125 MHz, DMSO): δ 14.5, 110.2, 122.3, 123.5, 129.6, 131.0, 134.2, 135.6, 141.4, 152.5, 159.4, 176.3; EIMS m/z (rel. int.) calcd for C₁₄H₁₁ClO₂ (M⁺, %): 246 (12).

3-(furan-2-yl)-1-(5-methylfuran-2-yl)prop-2-en-1-one (**2r**) Yield: 66%; brown crystals; IR(KBr) ν_{\max} : 2931 (C–H stretch), 1654 (C=O), 1514 (C=C), 1064, 1018; ^1H NMR (500 MHz, DMSO): δ 2.40 (s, 3H, CH₃), 6.41 (d, $J = 3.0$ Hz, 1H, H-4 furanyl), 6.67 (d, $J = 1.5$ Hz, 1H, H-3' furanyl), 7.04 (d, $J = 3.0$ Hz, 1H, H-5' furanyl), 7.30 (d, $J = 15.5$ Hz, 1H, H- α), 7.53 (d, $J = 15.5$ Hz, 1H, H- β), 7.58 (dd, $J = 3.0$ Hz/1.5 Hz, 1H, H-4' furanyl), 7.88 (d, $J = 3.0$ Hz, 1H, H-3 furanyl). ^{13}C NMR (125 MHz, DMSO): δ 14.4, 110.3, 113.8, 117.5, 119.4, 121.4, 129.5, 146.7, 151.7, 152.5, 159.1, 176.2; EIMS m/z (rel. int.) calcd for C₁₂H₁₀O₃ (M⁺, %): 202 (M⁺, 100).

1-(2,5-dimethylfuran-3-yl)-3-(2-hydroxyphenyl)prop-2-en-1-one (**3a**) Yield: 32%; yellow crystals; IR(KBr) ν_{\max} : 3306 (–OH), 1642 (C=O), 1576 (C=C), 1458 (C=C), 1229 (C–O aromatic), 1017, 755; ^1H NMR (500 MHz, CD₃OD): δ 2.27 (s, 3H, CH₃), 2.56 (s, 3H, CH₃), 6.43 (s, 1H, H-4 furanyl), 6.87 (overlapped, 2H, H-3/5 phenyl), 7.24

(t, $J = 8.0$ Hz, 1H, H-4 phenyl), 7.45 (d, $J = 15.5$ Hz, 1H, H- α), 7.59 (d, $J = 8.0$ Hz, 1H, H-6 phenyl), 8.00 (d, $J = 15.5$ Hz, 1H, H- β). ^{13}C NMR (125 MHz, CD_3OD): δ 11.9, 13.4, 105.7, 115.9, 119.7, 121.9, 122.9, 123.8, 129.3, 131.6, 139.5, 150.5, 157.6, 157.8, 187.8; EIMS m/z (rel. int.) calcd for $\text{C}_{15}\text{H}_{14}\text{O}_3$ (M^+ , %): 242 (M^+ , 26).

1-(2,5-dimethylfuran-3-yl)-3-(3-hydroxyphenyl)prop-2-en-1-one (3b) Yield: 84%; yellow crystals; IR(KBr) ν_{max} : 3392 (–OH), 1651 (C=O), 1583 (C=C), 1452 (C=C), 1399, 1231 (C–O aromatic), 1019, 783; ^1H NMR (500 MHz, CD_3OD): δ 2.27 (s, 3H, CH_3), 2.52 (s, 3H, CH_3), 6.41 (s, 1H, H-4 furanyl), 6.85 (dd, $J = 8.0$ Hz/1.5 Hz, 1H, H-5 phenyl), 7.17 (overlapped, 2H, H-2/4 phenyl), 7.18 (d, $J = 16.0$ Hz, 1H, H- α), 7.25 (d, $J = 8.0$ Hz, 1H, H-6 phenyl), 7.56 (d, $J = 16.0$ Hz, 1H, H- β). ^{13}C NMR (125 MHz, CD_3OD): δ 11.9, 13.4, 105.6, 114.6, 117.6, 119.9, 123.8, 129.9, 136.3, 143.3, 150.5, 157.9, 158.2, 186.8, 193.0; EIMS m/z (rel. int.) calcd for $\text{C}_{15}\text{H}_{14}\text{O}_3$ (M^+ , %): 242 (M^+ , 100).

1-(2,5-dimethylfuran-3-yl)-3-(4-hydroxyphenyl)prop-2-en-1-one (3c); Yield: 54%; yellow powder; IR(KBr) ν_{max} : 3216 (–OH), 1675 (C=O), 1606 (C=C), 1454 (C=C), 1292, 1219 (C–O aromatic), 1163, 833; ^1H NMR (500 MHz, CD_3OD): δ 2.29 (s, 3H, CH_3), 2.57 (s, 3H, CH_3), 6.51 (s, 1H, H-4 furanyl), 7.21 (d, $J = 15.5$ Hz, 1H, H- α), 7.58 (d, $J = 9.0$ Hz, 2H, H-3/5 phenyl), 7.65 (d, $J = 15.5$ Hz, 1H, H- β), 7.80 (d, $J = 9.0$ Hz, 2H, H-2/6 phenyl). ^{13}C NMR (125 MHz, CD_3OD): δ 11.9, 13.4, 105.6, 115.7, 120.7, 122.7, 126.5, 130.4, 132.3, 143.8, 150.5, 160.4, 191.7; EIMS m/z (rel. int.) calcd for $\text{C}_{15}\text{H}_{14}\text{O}_3$ (M^+ , %): 242 (M^+ , 100).

2-(2-(3-(2,5-dimethylfuran-3-yl)-3-oxoprop-1-enyl)phenoxy)acetic acid (3d) Yield: 42%; yellow powder; IR(KBr) ν_{max} : ^1H NMR (500 MHz, DMSO): δ 2.25 (s, 3H, CH_3), 2.25 (s, 3H, CH_3), 4.81 (s, 2H, CH_2), 6.75 (s, 1H, H-4 furanyl), 7.00 (overlapped, 2H, H-3/5 phenyl), 7.39 (t, $J = 8.0$ Hz, 1H, H-4 phenyl), 7.68 (d, $J = 15.5$ Hz, 1H, H- α), 7.80 (d, $J = 8.0$ Hz, 1H, H-6 phenyl), 7.87 (d, $J = 15.5$ Hz, 1H, H- β). ^{13}C NMR (125 MHz, DMSO): δ 13.6, 14.7, 65.6, 106.8, 113.2, 121.8, 123.1, 123.8, 125.8, 130.7, 132.3, 138.2, 150.4, 157.5, 157.7, 170.7, 185.9; EIMS m/z (rel. int.) calcd for $\text{C}_{17}\text{H}_{16}\text{O}_5$ (M^+ , %): 300 (M^+ , 48).

3-(2-hydroxyphenyl)-1-(pyridin-2-yl)prop-2-en-1-one (4a); Yield: 32%; green crystals; IR(KBr) ν_{max} : 3401 (–OH), 1660 (C=O), 1592 (C=C), 1458, 1339, 746; ^1H NMR (500 MHz, CD_3OD): δ 6.88 (dd, $J = 8.0$ Hz/1.5 Hz, 1H, H-3 phenyl), 6.90 (t, $J = 8.0$ Hz, 1H, H-5 phenyl), 7.26 (td, $J = 8.0$ Hz/1.5 Hz, 1H, H-4 phenyl), 7.59 (dd, $J = 8.0$ Hz/1.5 Hz, 1H, H-6 phenyl), 7.70 (d, $J = 15.0$ Hz, 1H, H- α), 8.00 (td, $J = 8.0$ Hz/1.5 Hz, 1H, H-5 pyridinyl), 8.14 (d, $J = 15.0$ Hz, 1H, H- β), 8.27 (overlapped, 2H, H-3/4 pyridinyl), 8.74 (dd, $J = 8.0$ Hz/1.5 Hz, 1H, H-6 pyridinyl). ^{13}C NMR (125 MHz,

CD_3OD): δ 116.0, 119.7, 120.1, 122.2, 122.8, 127.1, 128.8, 132.1, 137.6, 141.1, 148.9, 154.5, 157.8, 190.3; EIMS m/z (rel. int.) calcd for $\text{C}_{14}\text{H}_{11}\text{NO}_2$ (M^+ , %): 225 (M^+ , 15).

3-(3-hydroxyphenyl)-1-(pyridin-2-yl)prop-2-en-1-one (4b) Yield: 62%; pale green powder; IR(KBr) ν_{max} : 3326 (–OH), 1667 (C=O), 1581 (C=C), 1451, 1243 (C–O aromatic), 778; ^1H NMR (500 MHz, CD_3OD): δ 6.87 (dd, $J = 7.5$ Hz/1.5 Hz, 1H, H-4 phenyl), 7.15 (s, 1H, H-2 phenyl), 7.20 (d, $J = 7.5$ Hz, 1H, H-6 phenyl), 7.27 (t, $J = 7.5$ Hz, 1H, H-5 phenyl), 7.61 (td, $J = 7.5$ Hz/1.5 Hz, 1H, H-5 pyridinyl), 7.81 (d, $J = 16.0$ Hz, 1H, H- α), 7.98 (td, $J = 7.5$ Hz/1.5 Hz, 1H, H-4 pyridinyl), 8.14 (d, $J = 7.5$ Hz, 1H, H-3 pyridinyl), 8.20 (d, $J = 16.0$ Hz, 1H, H- β), 8.73 (dd, $J = 7.5$ Hz/1.5 Hz, 1H, H-6 pyridinyl). ^{13}C NMR (125 MHz, CD_3OD): δ 114.7, 118.0, 120.3, 120.7, 122.8, 127.3, 129.9, 136.5, 137.6, 145.1, 149.0, 154.2, 158.0, 199.7; EIMS m/z (rel. int.) calcd for $\text{C}_{14}\text{H}_{11}\text{NO}_2$ (M^+ , %): 225 (M^+ , 25).

3-(2-hydroxyphenyl)-1-(pyridin-4-yl)prop-2-en-1-one (5a) Yield: 31%; yellow crystals; IR(KBr) ν_{max} : 3273 (–OH), 1642 (C=O), 1586 (C=C), 1458, 1251 (C–O aromatic), 753; ^1H NMR (500 MHz, CD_3OD): δ 6.90 (d, $J = 8.0$ Hz, 1H, H-3 phenyl), 7.29 (t, $J = 8.0$ Hz, 1H, H-5 phenyl), 7.70 (d, $J = 8.0$ Hz, 1H, H-6 phenyl), 7.75 (d, $J = 16.0$ Hz, 1H, H- α), 7.88 (t, $J = 8.0$ Hz, 1H, H-4 phenyl), 7.93 (d, $J = 6.0$ Hz, 2H, H-3/5 pyridinyl), 8.17 (d, $J = 16.0$ Hz, 1H, H- β), 8.78 (d, $J = 6.0$ Hz, 2H, H-2/6 pyridinyl). ^{13}C NMR (125 MHz, CD_3OD): δ 116.0, 119.8, 120.8, 122.1, 123.0, 129.5, 132.5, 143.3, 150.1, 150.2, 163.9, 189.2; EIMS m/z (rel. int.) calcd for $\text{C}_{14}\text{H}_{11}\text{NO}_2$ (M^+ , %): 224 (M^+ , 13).

3-(3-hydroxyphenyl)-1-(pyridin-4-yl)prop-2-en-1-one (5b) Yield: 42%; pale yellow powder; IR(KBr) ν_{max} : 3436 (–OH), 1631 (C=O), 1580 (C=C), 1414, 1240 (C–O aromatic), 786; ^1H NMR (500 MHz, CD_3OD): δ 6.91 (d, $J = 8.0$ Hz, 1H, H-4 phenyl), 7.16 (s, 1H, H-2 phenyl), 7.24 (d, $J = 8.0$ Hz, 1H, H-6 phenyl), 7.28 (t, $J = 8.0$ Hz, 1H, H-5 phenyl), 7.61 (d, $J = 16.0$ Hz, 1H, H- α), 7.77 (d, $J = 16.0$ Hz, 1H, H- β), 7.95 (d, $J = 6.0$ Hz, 2H, H-3/5 pyridinyl), 8.78 (d, $J = 6.0$ Hz, 2H, H-2/6 pyridinyl). ^{13}C NMR (125 MHz, CD_3OD): δ 114.9, 118.3, 120.4, 121.0, 122.1, 129.9, 135.9, 145.3, 147.1, 150.2, 158.0, 189.9; EIMS m/z (rel. int.) calcd for $\text{C}_{14}\text{H}_{11}\text{NO}_2$ (M^+ , %): 225 (M^+ , 55).

3-(4-hydroxyphenyl)-1-(pyridin-4-yl)prop-2-en-1-one (5c) Yield: 61%; orange powder; IR(KBr) ν_{max} : 3286 (–OH), 1632 (C=O), 1573 (C=C), 1456, 1252 (C–O aromatic), 782; ^1H NMR (500 MHz, CD_3OD): δ 6.87 (d, $J = 8.5$ Hz, 2H, H-5/5 phenyl), 7.60 (d, $J = 15.5$ Hz, 1H, H- α), 7.72 (d, $J = 8.5$ Hz, 2H, H-2/6 phenyl), 7.92 (d, $J = 15.5$ Hz, 1H, H- β), 8.58 (d, $J = 7.0$ Hz, 2H, H-3/5 pyridinyl), 9.09 (d, $J = 7.0$ Hz, 2H, H-2/6 pyridinyl). ^{13}C NMR (125 MHz, CD_3OD): δ 115.8, 117.4, 122.7, 127.1,

130.8, 137.6, 145.7, 148.9, 160.7, 189.7; EIMS m/z (rel. int.) calcd for $C_{14}H_{11}NO_2$ (M^+ , %): 225 (M^+ , 100).

3-(2-hydroxyphenyl)-1-(thiophen-2-yl)prop-2-en-1-one (6a) Yield: 25%; yellow solid; IR(KBr) ν_{max} : 3293 (–OH), 1636 (C=O), 1570 (C=C), 1412, 1234 (C–O aromatic), 1063, 752; 1H NMR (500 MHz, CD_3OD): δ 6.89 (overlapped, 2H, H-3/5 phenyl), 7.25 (overlapped, 2H, H-4 thiophenyl/H-4 phenyl), 7.67 (d, $J = 8.0$ Hz, 1H, H-6 phenyl), 7.76 (d, $J = 15.5$ Hz, 1H, H- α), 7.86 (dd, $J = 4.5$ Hz/1.5 Hz, 1H, H-3 thiophenyl), 8.02 (dd, $J = 4.5$ Hz/1.5 Hz, 1H, H-5 thiophenyl), 8.15 (d, $J = 15.5$ Hz, 1H, H- β). ^{13}C NMR (125 MHz, CD_3OD): δ 115.9, 119.7, 121.1, 121.8, 129.4, 131.4, 131.9, 132.6, 134.4, 140.5, 145.7, 157.8, 183.7; EIMS m/z (rel. int.) calcd for $C_{13}H_{10}O_2S$ (M^+ , %): 230 (M^+ , 14).

3-(4-hydroxyphenyl)-1-(thiophen-2-yl)prop-2-en-1-one (6b) Yield: 71%; yellow powder; IR(KBr) ν_{max} : 3171 (–OH), 1671 (C=O), 1605 (C=C), 1454 (C=C), 1290 (C–O aromatic), 1219 (C–O), 1163, 833; 1H NMR (500 MHz, CD_3OD): δ 6.86 (d, $J = 8.5$ Hz, 2H, H-3/5 phenyl), 7.25 (t, $J = 4.0$ Hz, 1H, H-4 thiophenyl), 7.50 (d, $J = 15.5$ Hz, 1H, H- α), 7.61 (d, $J = 8.5$ Hz, 2H, H-2/6 phenyl), 7.76 (d, $J = 15.5$ Hz, 1H, H- β), 7.84 (dd, $J = 4.0$ Hz/1.5 Hz, 1H, H-3 thiophenyl), 8.05 (dd, $J = 4.0$ Hz/1.5 Hz, 1H, H-5 thiophenyl). ^{13}C NMR (125 MHz, CD_3OD): δ 115.8, 118.1, 126.4, 128.5, 130.8, 132.6, 134.3, 144.8, 145.8, 160.6, 183.2; EIMS m/z (rel. int.) calcd for $C_{15}H_{14}O_3S$ (M^+ , %): 230 (M^+ , 100).

3-(2,5-dimethoxyphenyl)-1-(thiophen-2-yl)prop-2-en-1-one (6c) Yield: 71%; yellow crystals; IR(KBr) ν_{max} : 2942 (C–H stretch), 1647 (C=O), 1589 (C=C), 1495 (C=C), 1414, 1258 (C–O aromatic), 1219 (C–O), 1044; 1H NMR (500 MHz, $CDCl_3$): δ 3.79 (s, 3H, OMe), 3.85 (s, 3H, OMe), 6.86 (d, $J = 9.0$ Hz, 1H, H-4 phenyl), 6.93 (d, $J = 9.0$ Hz, 1H, H-3 phenyl), 7.14 (s, 1H, H-6 phenyl), 7.16 (t, $J = 4.0$ Hz, 1H, H-4 thiophenyl), 7.51 (d, $J = 15.5$ Hz, 1H, H- α), 7.65 (d, $J = 4.0$ Hz, 1H, H-3 thiophenyl), 7.84 (d, $J = 4.0$ Hz, 1H, H-5 thiophenyl), 8.11 (d, $J = 15.5$ Hz, 1H, H- β). ^{13}C NMR (125 MHz, $CDCl_3$): δ 56.0, 56.4, 112.7, 114.2, 117.4, 122.9, 124.5, 128.4, 131.9, 133.8, 139.6, 146.0, 153.6, 153.7, 182.8; EIMS m/z (rel. int.) calcd for $C_{15}H_{14}O_3S$ (M^+ , %): 274 (M^+ , 10).

1-(5-chlorothiophen-2-yl)-3-(2-hydroxyphenyl)prop-2-en-1-one (7a) Yield: 51%; yellow needle crystals; IR(KBr) ν_{max} : 3258 (–OH), 1629 (C=O), 1565 (C=C), 1415, 1231 (C–O aromatic), 1021, 744; 1H NMR (500 MHz, CD_3OD): δ 6.89 (overlapped, 2H, H-3/5 phenyl), 7.14 (d, $J = 4.0$ Hz, 1H, H-4 thiophenyl), 7.28 (td, $J = 8.0$ Hz/2.0 Hz, 1H, H-4 phenyl), 7.67 (d, $J = 15.5$ Hz, 1H, H- α), 7.68 (dd, $J = 8.5$ Hz/2.0 Hz, 1H, H-6 phenyl), 7.87 (d, $J = 4.0$ Hz, 1H, H-3 thiophenyl), 8.14 (d, $J = 15.5$ Hz, 1H, H- β). ^{13}C NMR (125 MHz, CD_3OD): δ 115.9, 119.7,

121.7, 128.1, 128.3, 129.4, 132.1, 132.3, 139.2, 140.9, 144.9, 157.9, 182.6; EIMS m/z (rel. int.) calcd for $C_{13}H_9ClO_2S$ (M^+ , %): 264 (M^+ , 12).

1-(5-chlorothiophen-2-yl)-3-(3-hydroxyphenyl)prop-2-en-1-one (7b) Yield: 56%; pale yellow solid; IR(KBr) ν_{max} : 3370 (–OH), 1641 (C=O), 1582 (C=C), 1416, 1262 (C–O aromatic), 1022; 1H NMR (500 MHz, CD_3OD): δ 6.89 (dd, $J = 8.0$ Hz/1.0 Hz, 1H, H-4 phenyl), 7.12 (s, 1H, H-2 phenyl), 7.14 (d, $J = 4.0$ Hz, 1H, H-4 thiophenyl), 7.22 (dd, $J = 8.0$ Hz/1.0 Hz, 1H, H-6 phenyl), 7.27 (t, $J = 8.0$ Hz, 1H, H-5 phenyl), 7.55 (d, $J = 15.5$ Hz, 1H, H- α), 7.72 (d, $J = 15.5$ Hz, 1H, H- β), 7.93 (d, $J = 4.0$ Hz, 1H, H-3 thiophenyl). ^{13}C NMR (125 MHz, CD_3OD): δ 114.8, 118.0, 120.1, 120.2, 128.4, 129.9, 132.8, 136.1, 139.6, 144.6, 144.8, 157.9, 181.9; EIMS m/z (rel. int.) calcd for $C_{13}H_9ClO_2S$ (M^+ , %): 264 (M^+ , 50).

1-(5-chlorothiophen-2-yl)-3-(4-hydroxyphenyl)prop-2-en-1-one (7c) Yield: 71%; yellow powder; IR(KBr) ν_{max} : 3369 (–OH), 1676 (C=O), 1582 (C=C), 1416, 1217 (C–O aromatic), 1157; 1H NMR (500 MHz, CD_3OD): δ 6.85 (d, $J = 8.0$ Hz, 2H, H-3/5 phenyl), 7.11 (d, $J = 4.0$ Hz, 1H, H-4 thiophenyl), 7.43 (d, $J = 15.5$ Hz, 1H, H- α), 7.61 (d, $J = 8.0$ Hz, 2H, H-2/6 phenyl), 7.74 (d, $J = 15.5$ Hz, 1H, H- β), 7.88 (d, $J = 4.0$ Hz, 1H, H-3 thiophenyl). ^{13}C NMR (125 MHz, CD_3OD): δ 115.8, 116.7, 126.3, 128.2, 130.8, 132.2, 139.1, 144.9, 145.0, 160.8, 182.1; EIMS m/z (rel. int.) calcd for $C_{13}H_9ClO_2S$ (M^+ , %): 264 (M^+ , 100).

1-(5-chlorothiophen-2-yl)-3-(2,5-dimethoxyphenyl)prop-2-en-1-one (7d) Yield: 63%; yellow powder; IR(KBr) ν_{max} : 2923 (C–H stretch), 1676 (C=O), 1614 (C=C), 1511 (C=C), 1225 (C–O aromatic), 1074; 1H NMR (500 MHz, DMSO): δ 3.79 (s, 3H, CH_3), 3.83 (s, 3H, CH_3), 7.04 (overlapped, 2H, H-3/4 phenyl), 7.37 (d, $J = 4.0$ Hz, 1H, H-4 thiophenyl), 7.54 (s, 1H, H-6 phenyl), 7.80 (d, $J = 15.5$ Hz, 1H, H- α), 7.90 (d, $J = 15.5$ Hz, 1H, H- β), 8.24 (d, $J = 4.0$ Hz, 1H, H-3 thiophenyl). ^{13}C NMR (125 MHz, DMSO): δ 56.5, 56.9, 113.3, 113.8, 119.2, 121.2, 123.8, 129.7, 129.9, 134.4, 138.6, 145.4, 153.5, 153.9, 181.7; EIMS m/z (rel. int.) calcd for $C_{15}H_{13}ClO_3S$ (M^+ , %): 308 (M^+ , 11).

Bioassay procedures

Cell cultures and treatment

The RAW 264.7 cells (ATCC) were cultured in a plastic culture flask in Dulbecco's Modified Eagle's Medium (DMEM) supplemented with 10% FBS and 1% penicillin/streptomycin under 5% CO_2 atmosphere at 37°C. Cells at confluency of 80–90% were scrapped out and seeded into 96-well plate at 5×10^4 cells/50 μ l well. Attached cells were then induced with 100 U/ml of recombinant mouse

interferon-gamma (IFN- γ) and 5 $\mu\text{g/ml}$ of LPS (*Escherichia coli*, serotype 0111:B4) in the presence or absence (negative control) of test compounds for 17–20 h. The NO production was then determined by Griess assay, and the percentage of the activity was calculated.

Griess assay

The NO scavenging (Mirkov *et al.*, 2004) and NO production in cell culture were determined by measuring the nitrite (NO_2^-) formation in the SNP solution mixtures and supernatants of spent cell culture media, respectively, by using Griess assay (Tsikas, 2007). In brief, 50 μl of Griess Reagent (1% sulfanilamide and 0.1% naphthylethylenediamine dihydrochloride in 2.5% H_3PO_4) was added to 50 μl of SNP solution mixtures and/or cell culture supernatant. The color density was measured at 550 nm after 10 min incubation at room temperature.

Cell viability determination (MTT assay)

After removal of culture media, all wells were topped-up with 100 μl of DMEM, followed by the addition of 20 μl of 3-(4,5-dimethylthiazol-2-yl)-2,5-diphenyltetrazolium bromide (MTT, 5 mg/ml). The cells were incubated under 5% CO_2 at 37°C for 4 h. The formazan crystals formed were dissolved in DMSO, the absorbance was read at 570 nm, and the percentage of cell viability was calculated.

Statistical analysis

The IC_{50} values were calculated using GraphPad Prism software with one parameter model [$y = 100/(1 + a/x)$]. Differences between the groups were determined by one-way analysis of variance (ANOVA) followed by Dunnett test method. Statistical significance of differences between the groups was accepted at $P < 0.05$.

Computational procedures

Molecular modeling and alignment

All molecular modeling methods were performed using SYBYL 7.3 (Sybyl) on Genuine Intel® Xeon® 2.33 GHz Quadcore processor running under open SuSe Linux 11.0 environment. The 3D structures of all compounds were built and minimized with conjugate gradient's method using SYBYL 7.3 Tripos force field with 1000 iterations. The geometries of all molecules involved in this study were optimized by conjugate gradient's method using Tripos force field. Then, the common linker of the chalcone

skeleton was selected as the atoms to superimpose all the compounds using SYBYL 7.3 alignment method.

CoMFA analysis

The steric and electrostatic fields in CoMFA were calculated using sp^3 carbon atom with +1.0 charge as the probe atom. Both field energies were truncated to ± 30 kcal/mol, and the CoMFA fields generated automatically were scaled by the CoMFA-STD method. In order to investigate the effect of grid spacing, initially the CoMFA models were developed at varying grid spacing values (i.e., 0.5, 1.0 and 2.0 Å), and the best q^2 values were obtained when the grid spacing was set to 2.0 Å.

Partial least squares (PLS) analysis

The PLS method was employed to set up a correlation between the molecular fields and the pIC_{50} of anti-inflammatory activities of the tested compounds. The optimal number of components was determined using cross-validation (leave-one-out) method. To speed up the analysis and reduce noise, columns with an r value below 2.0 kcal/mol were filtered off. The cross-validated q^2 that resulted in optimum number of components and the lowest standard error of prediction were taken. Final analysis was then performed to calculate conventional r^2 and standard error using the optimum number of components.

CoMFA contour maps

Contour maps were generated as a scalar product of the coefficients and standard deviations ($\text{StDev} \times \text{Coeff}$) associated with each column. Favored and disfavored levels, fixed at 80 and 20%, respectively, were employed to display the steric fields are shown in green (more bulk favored) and yellow (less bulk favored), while the electrostatic field contours are displayed in red (electronegative substituents favored) and blue (electropositive substituents favored) colors.

Acknowledgment This study was financially supported by a grant from the Ministry of Higher Education, Malaysia under the Fundamental Research Grant Scheme (FRGS) (01-11-08-651FR). Kok-Wai Lam was a recipient of the Graduate Research Fellowship (GRF) scheme supported by UPM.

References

- Ahmad S, Israf DA, Lajis NH, Shaari K, Mohamed H, Wahab AA, Ariffin KT, Hoo WY, Aziz NA, Kadir AA, Sulaiman MR, Somchit MN (2006) Cardamonin, inhibits pro-inflammatory mediators in activated RAW 264.7 cells and whole blood. *Eur J Pharmacol* 538(1–3):188–194

- Balanco JM, Pral EM, da Silva S, Bijovsky AT, Mortara RA, Alfieri SC (1998) Axenic cultivation and partial characterization of *Leishmania braziliensis* amastigote-like stages. *Parasitology* 116(Pt 2):103–113
- Boeck P, Bandeira Falcao CA, Leal PC, Yunes RA, Filho VC, Torres-Santos EC, Rossi-Bergmann B (2006) Synthesis of chalcone analogues with increased antileishmanial activity. *Bioorg Med Chem* 14(5):1538–1545
- Chen M, Christensen SB, Theander TG, Kharazmi A (1994) Antileishmanial activity of licochalcone A in mice infected with *Leishmania major* and in hamsters infected with *Leishmania donovani*. *Antimicrob Agents Chemother* 38(6):1339–1344
- Chiaradia LD, dos Santos R, Vitor CE, Vieira AA, Leal PC, Nunes RJ, Calixto JB, Yunes RA (2008) Synthesis and pharmacological activity of chalcones derived from 2,4,6-trimethoxyacetophenone in RAW 264.7 cells stimulated by LPS: quantitative structure-activity relationships. *Bioorg Med Chem* 16(2):658–667
- Cooke SA, Corlett GK, Legon AC (1998) Rotational spectrum of thiophene? HCl. Does thiophene act as an aromatic *p*-type electron donor or an *n*-type electron donor in hydrogen-bond formation? *J Chem Soc Faraday Trans* 94(11):1565–1570
- Correa R, Pereira MA, Buffon D, dos Santos L, Cechinell Filho V, Santos AR, Nunes RJ (2001) Antinociceptive properties of chalcones. Structure-activity relationships. *Arch Pharm (Weinheim)* 334(10):332–334
- Cramer Iii RD, Patterson DE, Bunce JD (1988) Comparative molecular field analysis (CoMFA). 1. Effect of shape on binding of steroids to carrier proteins. *J Am Chem Soc* 110(18):5959–5967
- Huang YC, Guh JH, Cheng ZJ, Chang YL, Hwang TL, Lin CN, Teng CM (2001) Inhibitory effect of DCDC on lipopolysaccharide-induced nitric oxide synthesis in RAW 264.7 cells. *Life Sci* 68(21):2435–2447
- Israf DA, Khaizurin TA, Syahida A, Lajis NH, Khozirah S (2007) Cardamonin inhibits COX and iNOS expression via inhibition of p65NF- κ B nuclear translocation and I κ -B phosphorylation in RAW 264.7 macrophage cells. *Mol Immunol* 44(5):673–679
- Ko HH, Tsao LT, Yu KL, Liu CT, Wang JP, Lin CN (2003) Structure-activity relationship studies on chalcone derivatives: the potent inhibition of chemical mediators release. *Bioorg Med Chem* 11(1):105–111
- Liew CY, Tham CL, Lam KW, Mohamad AS, Kim MK, Cheah YK, Zakaria ZA, Sulaiman MR, Lajis MN, Israf DA (2010) A synthetic hydroxypropenone inhibits nitric oxide, prostaglandin E2, and proinflammatory cytokine synthesis. *Immunopharmacol Immunotoxicol* 32:495
- Lipinski CA, Lombardo F, Dominy BW, Feeney PJ (2001) Experimental and computational approaches to estimate solubility and permeability in drug discovery and development settings. *Adv Drug Deliv Rev* 46(1–3):3–26
- Liu X, Go ML (2007) Antiproliferative activity of chalcones with basic functionalities. *Bioorg Med Chem* 15(22):7021–7034
- Lopez SN, Castelli MV, Zacchino SA, Dominguez JN, Lobo G, Charris-Charris J, Cortes JC, Ribas JC, Devia C, Rodriguez AM, Enriz RD (2001) In vitro antifungal evaluation and structure-activity relationships of a new series of chalcone derivatives and synthetic analogues, with inhibitory properties against polymers of the fungal cell wall. *Bioorg Med Chem* 9(8):1999–2013
- Mirkov SM, Djordjevic AN, Andric NL, Andric SA, Kostic TS, Bogdanovic GM, Vojinovic-Miloradov MB, Kovacevic RZ (2004) Nitric oxide-scavenging activity of polyhydroxylated fullereneol, C60(OH)24. *Nitric Oxide* 11(2):201–207
- Phrutivorapongkul A, Lipipun V, Ruangrunsi N, Kirtikara K, Nishikawa K, Maruyama S, Watanabe T, Ishikawa T (2003) Studies on the chemical constituents of stem bark of *Millettia leucantha*: isolation of new chalcones with cytotoxic, anti-herpes simplex virus and anti-inflammatory activities. *Chem Pharm Bull (Tokyo)* 51(2):187–190
- Rojas J, Dominguez JN, Charris JE, Lobo G, Paya M, Ferrandiz ML (2002) Synthesis and inhibitory activity of dimethylamino-chalcone derivatives on the induction of nitric oxide synthase. *Eur J Med Chem* 37(8):699–705
- Sivakumar PM, Seenivasan SP, Kumar V, Doble M (2007) Synthesis, antimycobacterial activity evaluation, and QSAR studies of chalcone derivatives. *Bioorg Med Chem Lett* 17(6):1695–1700
- Tetko IV, Gasteiger J, Todeschini R, Mauri A, Livingstone D, Ertl P, Palyulin VA, Radchenko EV, Zefirov NS, Makarenko AS, Tanchuk VY, Prokopenko VV (2005) Virtual computational chemistry laboratory—design and description. *J Comput Aided Mol Des* 19(6):453–463
- Tsikas D (2007) Analysis of nitrite and nitrate in biological fluids by assays based on the Griess reaction: appraisal of the Griess reaction in the L-arginine/nitric oxide area of research. *J Chromatogr B Analyt Technol Biomed Life Sci* 851(1–2):51–70
- Veber DF, Johnson SR, Cheng HY, Smith BR, Ward KW, Kopple KD (2002) Molecular properties that influence the oral bioavailability of drug candidates. *J Med Chem* 45(12):2615–2623
- Won SJ, Liu CT, Tsao LT, Weng JR, Ko HH, Wang JP, Lin CN (2005) Synthetic chalcones as potential anti-inflammatory and cancer chemopreventive agents. *Eur J Med Chem* 40(1):103–112
- Xue CX, Cui SY, Liu MC, Hu ZD, Fan BT (2004) 3D QSAR studies on antimalarial alkoxyated and hydroxylated chalcones by CoMFA and CoMSIA. *Eur J Med Chem* 39(9):745–753